

SQLR: Short Term Memory Q-Learning for Elastic Provisioning

Constantine Ayimba, *Student Member, IEEE*, Paolo Casari, *Senior Member, IEEE*
and Vincenzo Mancuso, *Member, IEEE*

Abstract—As more and more application providers transition to the cloud and deliver their services on a Software as a Service (SaaS) basis, cloud providers need to make their provisioning systems agile enough to deliver on Service Level Agreements. At the same time they should guard against over-provisioning which limits their capacity to accommodate more tenants. To this end we propose SQLR, a dynamic provisioning system employing a customized model-free reinforcement learning algorithm that is capable of reusing contextual knowledge learned from one workload to optimize resource provisioning for different workload patterns. SQLR achieves results comparable to those where resources are unconstrained, with minimal overhead. Our experiments show that we can reduce the amount of resources that need to be provisioned by almost 25% with less than 1% overall service unavailability due to blocking, and still deliver similar response times as an over-provisioned system.

Index Terms—NFV, Provisioning, SLA, CSP, Horizontal scaling, Q-Learning, Cloud economics

1 INTRODUCTION

The popularity of cloud networks as the preferred medium to provide services to end users has resulted in Cloud Service Providers (CSPs) facing increasing demands on finite resources with high expectations on performance by Application Service Providers (ASPs) [1]. CSPs must therefore balance the need for high Quality of Service (QoS) guarantees with just the right amount of resources, so that cloud services can be cost-effectively delivered without violating such Service Level Objectives (SLOs) as response time or service availability.

SLO violations can have serious consequences for ASPs such as loss of users and related revenue loss [2]. In many cases, this also results in the CSP paying penalties to the ASP [3]. For CSPs, this creates the need for dynamic provisioning (scaling) tools. Such tools increase the resources allocated to an application when sudden increases in demand occur (or are foreseen) and release them when they are not needed. These actions both save costs for the ASPs and free capacity for other tenants of the CSPs.

Most state-of-the-art solutions to this problem leverage the continuous monitoring of application and system metrics to guide scaling decisions. This means that any significant modification to the application necessitates a reconfiguration of the dynamic scaling system.

To address this challenge we have developed an application-agnostic system which leverages model-free reinforcement learning to make the most favorable scaling decisions in the face of variable demand. Owing to the

fact that workload profiles tend to be stochastic over short intervals, reinforcement learning lends itself well to this problem, given its ability to learn from experience rather than from previously known data-sets. Concretely, our main contributions are:

- 1) A flexible scaling agent that
 - is horizontal, i.e., adapts the number of virtual machines (VMs) allocated to a service, not the resources (e.g. virtual CPUs or memory) assigned to them;
 - given high-level objectives, learns the optimal trade-off between the accepted level of service availability and the corresponding resource costs, and provisions accordingly amid challenging workloads;
 - adapts to different workloads by learning policies based on their resource utilization patterns and not on the workloads *per se*;
 - is application-agnostic, given its foundation on utilization metrics and not directly on expected response times;
 - progressively improves with every scaling decision resulting in better performance with regard to service reliability and availability.
- 2) A configuration-agnostic Admission Control Virtual Network Function (VNF) based on Q-Learning, that learns the most suitable action to take given the level of resource utilization reported by a Virtual Machine (VM) instance.
- 3) A weighted fair learning mechanism that encourages exploration in unfamiliar “states” and exploitation for better known states, thus increasing the likelihood of optimal actions even before convergence, when the system is still acting according to partially developed policies.

- C. Ayimba is with IMDEA Networks Institute and Universidad Carlos III de Madrid (UC3M), Madrid, Spain.
E-mail: constantine.ayimba@imdea.org
- P. Casari is with IMDEA Networks Institute, Madrid, Spain.
E-mail: paolo.casari@imdea.org
- V. Mancuso is with IMDEA Networks Institute, Madrid, Spain.
E-mail: vincenzo.mancuso@imdea.org

Unlike conventional reinforcement learning systems which are fully Markovian, our system uses a modified Q-Learning mechanism which keeps track of both the previous and current state which we define in terms of VM utilization levels and number of active VMs. This modification makes it possible for it to learn different policies for different traffic profiles by implicitly introducing the magnitude of state change as a distinguishing parameter between profiles.

The rest of this article is organized as follows: Section 2 examines prior approaches to scaling of cloud resources while in Section 2 we discuss the adaptations we made to conventional Q-Learning to achieve a short-term memory algorithm capable of learning multiple policies. In Section 4 we outline the experiments made to test the scaling and admission control algorithms. We discuss the results of our approach compared to other state-of-the-art methods in Section 5. In Section 6 we provide the main conclusions and discuss future directions along this line of research.

2 RELATED WORK

The most commonly used approaches in making automated scaling decisions are rule-based schemes. These approaches rely on leveraging resource utilization thresholds which can be fixed such as in commercial tools as Rightscale [4] and Amazon's EC2 [5] or loosely defined as the fuzzy logic variants proposed by [6], [7], [8] among others. These methods require sufficient knowledge of the cloud application in order to define the operating bounds correctly.

The authors of [9] propose a theoretical model based reinforcement learning approach to cloud resource allocation, which takes into account net gains for the CSP as well as SLO violations. Their modelling, however assumes high predictability in arrival rates and system responses, both of which are highly stochastic in real environments.

The authors of [10] use a combination of a queue model and Extended Kalman Filtering (EKF) to carry out horizontal scaling, i.e. the addition or removal of VMs to a resource pool providing a given service. They use a 3-tier cloud application with 3 classes of requests to generate the measurement model. The model, enhanced by EKF, estimates response times given the workload as input. Finally the response time estimates act as triggers for horizontal scaling.

Other methods seek to characterize the workload and make resource allocations accordingly. In [11], Vasic *et al.* classify workloads based on recurring patterns. Optimized resource allocations for these patterns are derived and re-used every time the patterns are detected in a new workload.

In order to carry out vertical scaling (the addition of system resources e.g. virtual CPUs on VMs while they are running), Ibidunmoye *et al.* [12] use a modified Q-Learning scheme with a state space based on a fuzzy logic combination of response times and utilization levels. They employ several cooperating agents to simultaneously explore the state space in order to speed up convergence to a given policy.

In [13], a scheme based on Q-Learning and heuristics is proposed that initially over-provisions resources when an

increase in the workload is detected, and then gradually de-allocates them. The objective of this scheme is to reduce SLO violations that occur when the workload increases suddenly but resources are added conservatively.

In [14], the authors propose a system which profiles resource capacities, predicts the subsequent workload pattern over a monitoring window and scales the system accordingly based on a trade-off between scaling costs and SLOs.

In [15], the provisioning problem is considered in terms of costs for the provider. The authors propose a system that schedules resources in a bid to minimize the costs incurred due to SLO violations and those resulting from leasing cloud resources. This work assumes that such costs are known well in advance, and that Billing Time Units (BTUs) for leasing resources are both coarse-grained (in the order of hours) and fixed. However, recent proposals on cloud brokerage [16] promise greater flexibility by making BTUs much more fine grained providing better cost-effectiveness for tenants with short-lived requirements. Whereas rule-based schemes are simple and easy to implement, setting the correct thresholds requires specialized cloud application domain knowledge and sufficient awareness of resources. Other state-of-the-art scaling methods require that the service response times, the workload, or both are continuously monitored and measured. In many cases, obtaining such data requires real-time analysis of logs, which may lead to significant overhead in large-scale systems. Workloads in particular may also vary wildly [17] resulting in premature scaling directives. Our scheme, instead, infers the changes in workload by monitoring how the system responds to it. This provides a more robust basis for decision-making, even in large deployments. Different workloads trigger distinct state transition sequences, resulting in new policies being learned, in addition to those already learned. Given this, the system will scale appropriately for future workloads that exhibit combinations of the already observed patterns without need for further training.

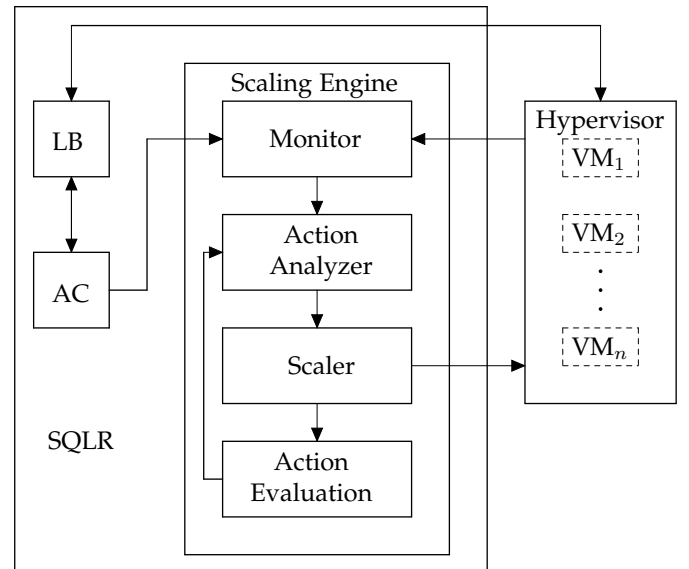


Fig. 1. SQLR block diagram. "LB" is the Load Balancer VNF and "AC" is the Admission Control VNF.

3 SYSTEM DESCRIPTION

A block diagram of the provisioning system we have developed (SQLR) is shown in Fig. 1. It comprises: a Load Balancer (LB) Virtual Network Function (VNF) coupled with an Admission Control (AC) VNF and a scaling engine. The latter leverages model-free reinforcement learning with inputs from system monitors in order to determine the appropriate horizontal scaling action. It then issues directives to the hypervisor to instantiate or shut down the VMs that deliver a cloud application as a service. We choose as our cloud application the double 256-bit hashing algorithm used for proof-of-work generation in bit-coin mining [18]. It is a suitable stand-in for resource-hungry, computationally challenging tasks that are commonly deferred to the cloud such as encryption [19] and transcoding [20], [21].

In a manner similar to the approach taken by [9], we treat admission control and horizontal scaling as sequential decisions. Such decisions can be formalised as Markov Decision Processes (MDPs) with a set of actions A , states S , state transition probabilities T and a reward function R .

$$\{T, S, A, R\}. \quad (1)$$

Further, we can consider the admission control and scaling mechanism as agents capable of epochal or episodic reinforcement learning. An episode or epoch consists of an agent observing its state, taking a given action permissible in that state, monitoring the environment to obtain the reward value corresponding to that action, and transitioning to a new state.

For an admission control agent, the permissible actions are to accept or drop a request. Moreover, by defining the state as the utilization level of the VM node handling the request, an accept or drop action results in a VM transitioning from one state to another with some probability. We structure the reward values based on how stable the resulting state is with respect to service times.

For the horizontal scaling agent, the actions are increasing, decreasing or maintaining the number of VMs. The state, in this case, is defined by three values: the system wide utilization before the action; the utilization after the action; and the number of active VMs. Therefore, the actions taken by the scaling agent results in a change in this set of values, which can be considered a transition in system state. We structure the reward function to include both the resulting blocking rate and the consequent number of VMs used.

By tracking how much reward an action receives and obtaining the state transition probabilities, the optimal actions (that yield the highest accumulated reward given a particular system state) can be determined, and the agent programmed to carry it out. However, a solution to the MDP is impractical given that the transition probabilities can vary widely depending on the workload and configuration of the system. A practical way that has been applied in many similar cases, where an exact solution to the MDP is intractable, is Q-Learning [22]. In this method, the agent develops a mapping of states to actions (known as the Q function) by tracking the accumulated reward or Q -value for each state-

action pair. Eventually it approximates the optimal action-value function q^* as: [23]:

$$\begin{aligned} Q(S^{(t)}, A^{(t)}) &\leftarrow \alpha R' + (1 - \alpha)Q(S^{(t)}, A^{(t)}) \\ R' &= R^{(t+1)} + \gamma \max_a Q(S^{(t+1)}, a), \end{aligned} \quad (2)$$

where at epoch t , the action-value is $Q(S^{(t)}, A^{(t)})$, and the immediate reward $R^{(t+1)}$ is what the agent receives after taking action a and ending up in state $S^{(t+1)}$, whose action-value is $Q(S^{(t+1)}, a)$. The fraction γ anticipates the contribution that future rewards will make towards the immediate one [22].

The use of a fixed learning rate α in (2) assumes that all states are visited evenly during training [23]. Depending on the formulation of the state space, this may not always be the case. Further, the update process given by (2) typically leads to a stochastic policy with values oscillating slightly about an estimated expected value. To ameliorate this effect, a modified reward mechanism can be used which takes into account the number of times the given state is visited. This method follows closely the algorithm for the online computation of the mean given in equation (3):

$$\begin{aligned} \mu_n &= \frac{1}{n} \sum_{k=1}^n (X_k) \\ &= \frac{1}{n} (X_n + (n-1)\mu_{n-1}). \end{aligned} \quad (3)$$

The Q function update then becomes:

$$Q(S^{(t)}, A^{(t)}) \leftarrow \frac{1}{n} [R' + (n-1)Q(S^{(t)}, A^{(t)})], \quad (4)$$

where n is the number of episodes (prior to the current action) that the agent acted with $(S^{(t)}, A^{(t)})$ as the preceding state-action pair. The modified update outlined in (4) also guarantees that a stationary policy will be developed given that the update value on the Right Hand Side becomes progressively smaller as the number of episodes increases.

Given that instantaneous reward values may be noisy owing to unforeseen effects of an action, we introduce a further modification to (4) which reduces the chances of wrongly estimating the mean action value at the initial learning phases:

$$\begin{aligned} Q(S^{(t)}, A^{(t)}) &\leftarrow \frac{1}{n} [\Delta + (n-1)Q(S^{(t)}, A^{(t)})], \\ \Delta &= R' - Q(S^{(t)}, A^{(t)}) \end{aligned} \quad (5)$$

The agent is trained by initially encouraging random actions (exploration). As it develops a policy, it progressively acts less randomly by choosing the actions yielding the highest reward at a given system state (exploitation). This is accomplished by employing ϵ -greedy action selection [23]. In this scheme, the action that yields the highest reward is chosen with a probability $(1-\epsilon)$ and a random action chosen with a probability ϵ .

Owing to the fact that not all states are visited with the same frequency, a global assignment and decrease of ϵ may bias the learned policy towards the most visited states. Therefore, we employ a scheme that reduces ϵ independently for each state depending on the number of times, i , that it is visited. This accelerates the learning process as well as performance, with regard to optimal action selection,

by encouraging exploration for the least visited states and exploitation for the most visited states. Specifically,

$$\epsilon = \begin{cases} 1 - \frac{i}{N}, & \text{if } i < N \\ \epsilon_{\min}, & \text{if } i \geq N, \end{cases} \quad (6)$$

where N is a setting of statistically significant visits, given the action space, that should result in convergence to a policy. A state is considered to have achieved convergence when its associated $\epsilon = \epsilon_{\min}$.

In order for the system to perform satisfactorily even before it has fully converged, we devise a weighted fair guided exploration scheme. In this scheme, at learning instance i , the probability $P^{(i)}$ of selecting an action a depends on its present action value $Q^{(i)}(s, a)$ and the number of times $n^{(i)}$ that it has been selected when the system is in state s :

$$P^{(i)} = \begin{cases} \frac{1}{L}, & \text{for } i = 0 \\ \frac{\Psi^{(i)}(1 - \tanh \phi^{(i)})}{\sum_{k=1}^L \Psi_k^{(i)}(1 - \tanh \phi_k^{(i)})}, & \text{for } i > 0 \end{cases} \quad (7)$$

$$\Psi^{(i)} = Q^{(i)}(s, a) + \sum_{j=1}^L |Q_k^{(i)}(s, a)|,$$

$$\phi^{(i)} = \frac{n^{(i)}}{i},$$

where L is the size of the action space. Given that $\Psi^{(i)} > 0$ it is used in place of the action value $Q^{(i)}(s, a)$ which, if negative, results in unfeasible probabilities. The hyperbolic tangent is a suitable weighing function, given that $0 \leq \tanh(\phi) \leq 1$ for $\phi \geq 0$.

In this way, a workable compromise between exploration and exploitation is achieved, curtailing the detrimental effects of unguided exploration on performance.

3.1 Admission Control and Load Balancer

In a resource-constrained system, an admission control mechanism ensures that the system does not take on more tasks than it can satisfactorily handle. Additionally, a load balancer ensures that the admitted load is apportioned well among the available resources in order to obtain good responses. The size of the action space for the admission control agent is two:

- 1) admit request;
- 2) drop request.

The state space, however, has to be derived from the levels of resource utilization on the VM that is serving the request. In this work, the resource considered is CPU utilization, as it is a low-level metric that correlates well with the workload, and it does not require any domain-specific knowledge of the deployed application [13]. Bearing in mind that response times are greatly impacted by how busy the system is, the upper threshold on utilization is chosen as the one beyond which the service times will violate the agreed SLO. This threshold is used as a target to determine the rewards/penalties the admission controller will accrue as it builds a policy using Q -Learning.

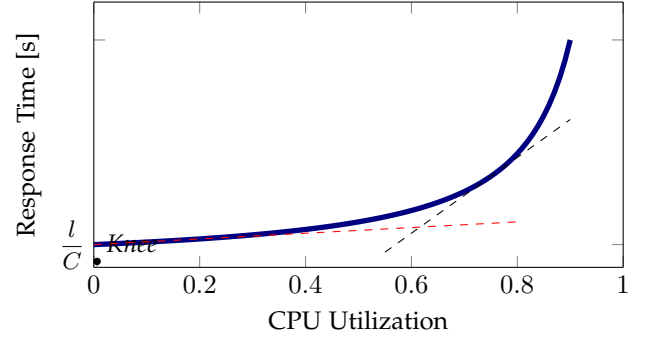


Fig. 2. Response time variation with load based on the queuing theory analysis presented in [24]. The variation is approximately linear just below the “knee”. If utilization levels are kept below this value, response times are most likely to be predictable/reliable.

The CPU utilization threshold is chosen based on the analytical results relating response times to occupancy in a processor sharing queue described in [24]. The time T , taken by a processor with capacity C operations per second to service a request requiring ℓ operations is given by:

$$T(\rho) = \frac{\ell}{C - \rho}, \quad (8)$$

$$\rho = \frac{\lambda}{\mu},$$

where λ , is the arrival rate (workload) and μ is the departure rate. The occupancy of the processor ρ is here considered as its utilization level.

The plot of (8) is given in Fig. 2. The point at which the gradient of the curve changes from an almost constant value to an exponential rise is chosen as the threshold beyond which service times become unpredictable/unreliable. We choose this by taking the intersection of the tangent to the curve at the point where the gradient is approximately 0.5s per 1% utilization with the tangent to the curve at the initial point with 0% utilization. This queuing theory result, though based on the assumption of Poisson distribution of arrivals, fits well with our experimental observations made with high entropy in arrival rate. An example of such an observation is depicted in Fig. 3, where service times are relatively constant around 1.2 s for utilization values lower than 62%, but vary wildly for higher levels.

In order to obtain a discretized state space, we partition those utilization values within which response times are predictable into regions. To this end, we employ the geometric quantizing function

$$x_j = \left\lfloor \left(1 - \left(\frac{1}{2} \right)^j \right) x_{\text{tgt}} \right\rfloor, j = 0, 1, \dots, n. \quad (9)$$

We define x_{bnd} as the boundary between the predictable and unpredictable regions with a value of 62%. In order to ensure that our admission policy keeps the system within the predictable region, we choose a training target, x_{tgt} , of 60% which is lower than the above upper bound. With x_n being the quantization level closest to the bound, we have that $x_n < x_{\text{tgt}} < x_{\text{bnd}}$. Operating a VM beyond this region is likely to result in service times that violate SLOs.

The expression for x_j is chosen given its characteristic of assigning large values at the initial stages and reducing

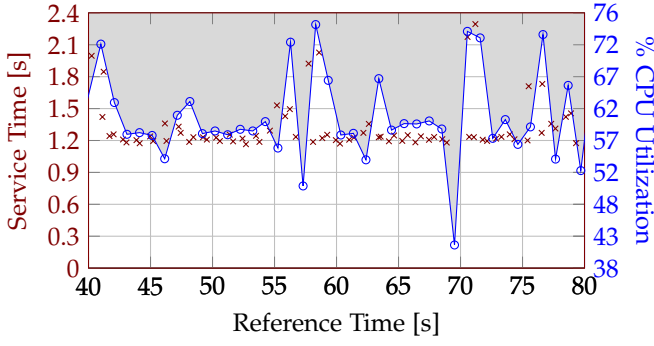


Fig. 3. Influence of CPU utilization on service response times.

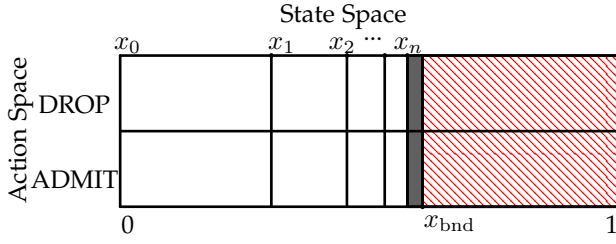


Fig. 4. Q function Table for training the AC. The gray area represents the ideal operating region at which resources are highly utilized and the service times are within SLOs. The red-shaded area on the right represents the region where VM operation is likely to cause SLO violations.

them as the threshold is approached. In this way a coarse and fine adjustment is achieved so that the practical utilization level learned by the system, x_{lim} , will be as high as possible.

The immediate reward, R , for the action taken by the admission controller is the resulting utilization, x , discretized to the nearest quantized level boundary (downwards for a DROP decision or upwards for an ADMIT decision). We do this in order to reduce the variance in the reward values assigned so as to accelerate convergence to a given policy. Therefore, with reference to Fig. 4, the reward is calculated as:

$$R(x) = \begin{cases} x_k, & \text{if } DROP \\ x_{k+1}, & \text{if } ADMIT, k = 0, 1, \dots, n \end{cases}$$

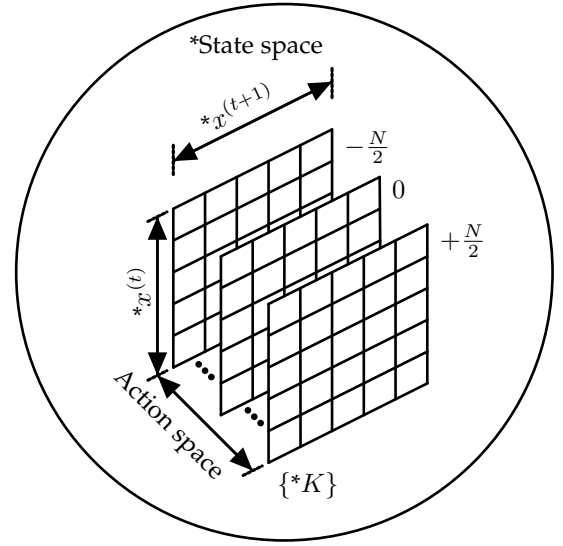
At the boundary $x_k = x_n, x_{k+1} = x_{bnd}$. Beyond the boundary, when $x > x_{bnd}$ $R(x)$ is defined as,

$$R(x) = \begin{cases} x_{bnd}, & \text{if } DROP \\ \frac{1}{2}(x_{bnd} - 1), & \text{if } ADMIT, \end{cases}$$

Note that for cases when $x > x_{bnd}$, the reward value for ADMIT is negative, implying a penalty for violating the allowable CPU utilization limit.

3.2 SQLR horizontal scaling agent

We design and implement a Q-Learning scaling agent, from this point on referred to as SQLR, whose objective is to achieve as low a blocking rate as possible with as few resources as possible. SQLR adds VM nodes (scale-out) or removes VM nodes (scale-in) as appropriate given the recent

Fig. 5. SQLR action and state space. K is the current number of active VM nodes, N is the range of VMs that can be added or removed. The state space, whose parameters are prefixed by (*), comprises the number of active VMs and the quantization levels of the average CPU utilization for the set of active VMs.

history of utilization experienced by the entire set of active VM nodes.

The state and action degrees of freedom for the horizontal scaling agent SQLR are as shown in Fig. 5. Each permissible action is represented as a “card” indicating the number of VMs that need to be added or removed in case of taking the action associated with the card. Moreover, each card consists of a grid whose rows and columns are indexed with load levels (to be interpreted as the immediate past and current episode’s load respectively) as highlighted in Fig. 6. The cells contain the cumulative reward obtained by a given state-action pair. We use a uniform quantizer for the state space since it provides a more granular view of the level of system-wide resource utilization than the geometric quantizer used for the admission control agent. However, because the context of a given utilization level is provided by how many active nodes are considered, greater nuance is required to distinguish the state space, particularly at the lower levels. To do so, we choose smaller steps (2%) in the region between 0-20% of utilization and 5% in the region between 20% and x_{lim} . The region above x_{lim} is chosen as one large level given that at this region of utilization a coarse scaling decision is most likely and, as such, it does not require a high resolution in the state space.

3.2.1 The Action Space

The scaling reward function (R_{sqlr}) consists of two components: R_{blk} computed using the blocking probability (P) and R_{res} computed from the resource cost (dependent on the number of active VM Nodes, K).

$$\begin{aligned} R_{sqlr} &= R_{blk} + R_{res} \\ R_{blk} &= \begin{cases} R_{min}, & \text{if } P \leq \bar{P} \\ \theta(\bar{P} - P), & \text{if } P > \bar{P}, \end{cases} \\ R_{res} &= \beta(1 - K) \end{aligned} \quad (10)$$

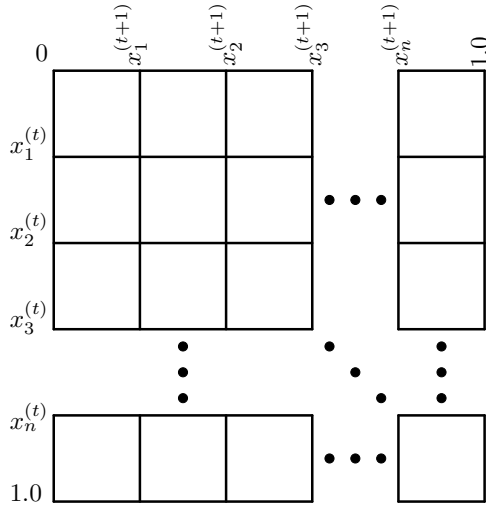


Fig. 6. State space detail for a “card” in the action space. Each cell’s index pair is given by the quantized level of average system-wide resource utilization in successive episodes.

where \bar{P} is the ideal blocking probability threshold and R_{\min} is a small positive reward given to the agent as an incentive for keeping the system within the allowable service outage limits. The training parameters θ and β act as modifiers, so that blocking probability violations receive a different penalty than that brought about by usage of extra resources. The reason is that the financial penalties incurred by a CSP for violating SLOs may be different from cost savings made by reducing resource usage.

3.2.2 The State Space

As stated earlier, each card in the bubble shown in Fig. 5 consists of a grid whose cell position indicators correspond to the average level of utilization of the active VMs before and after a scaling operation as shown in Fig. 6. The diagonal elements for the cases where the number of VM nodes remain unchanged (card “0” in Fig. 5) are initialized as non-zero values based on the cost associated with the number of active nodes and estimated values of blocking probability derived from the error function as shown in Fig. 7.

$$P_0(x) = \begin{cases} 0, & x < x_{\lim} \\ 1, & x > x_{\text{bnd}} \\ \frac{1}{2} \left[1 + \text{erf} \left(\eta(x) \frac{e}{\sqrt{2}} \right) \right], & \text{otherwise} \end{cases}$$

$$\eta(x) = \frac{x - x_{\lim}}{x_{\text{bnd}} - x_{\lim}}$$

These diagonal elements serve as the reference action values, $Q(S^{(t+1)}, a)$, for the updates in (5) after horizontal scaling. This process is depicted in Fig. 8 for a scale-out action. To describe this, we consider starting after an episodic wait period, the previous action having taken place at instant $t - 1$. At instance t , with K VMs, our scaler obtains the quantized level of the average utilization in the interval $[t - 1, t)$. This serves as the second member of the cell position indicator to be considered in selecting the action. The first member of the cell position indicator is the quantized

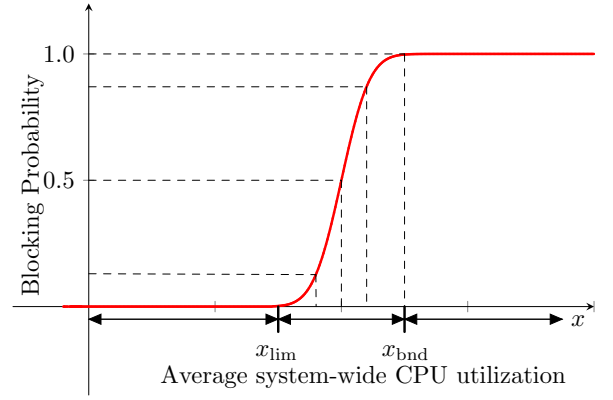


Fig. 7. Modified error function to estimate the blocking probability component of the initial Q values of card “0” (Fig. 5) diagonals.

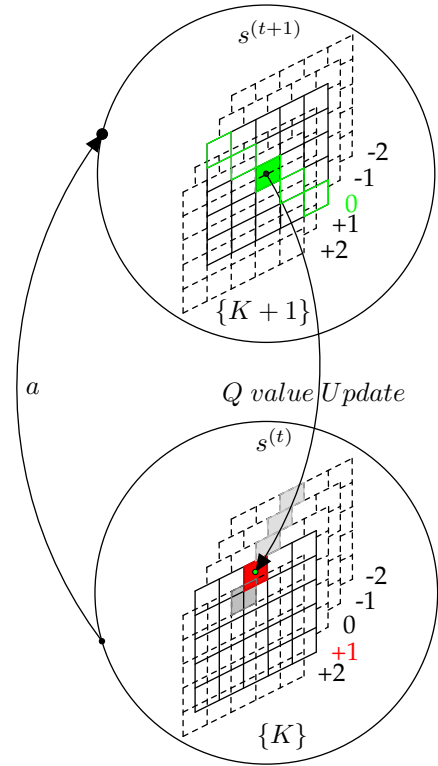


Fig. 8. SQLR horizontal scaling mechanism. The grey-shaded cells are those whose Q -values are compared to determine the action to take according to (7). A scale OUT of “+1” is chosen as the action. After scaling action a , the Q -value in the red-shaded cell receives the update as specified by (5). One component of the update is the Q -value contained in the green-shaded cell of card “0” in bubble “{ $K + 1$ }”.

level of the average utilization in the interval $[t - 2, t - 1)$. Given this triplet of values, the state is established. Then, by leveraging the Q -value entries of the cells with this reference set of position indicators in every card of the action space in the bubble defined by K VM nodes, a scaling action is chosen based on (7).

For later reference we term this cell, in the chosen action card, as R-Cell (marked red in Fig. 8). After waiting a short period for the VMs to start-up or shut-down a further

predefined wait period between episodes is observed to allow the effect of the change to be manifest. We are now at instant $t + 1$. The immediate reward value is then calculated taking account of the blocking probability observed between time instants t and $t + 1$ and the number of active VMs at instant $t + 1$ as described in (10). We also take into account the accumulated reward stored in card “0” with the diagonal cell whose two indicators are both given by the quantized average utilization values in the interval $[t, t + 1)$ (marked green in Fig. 8). These two values are used to update the value in R-Cell as prescribed in (5).

4 EXPERIMENTAL SETUP

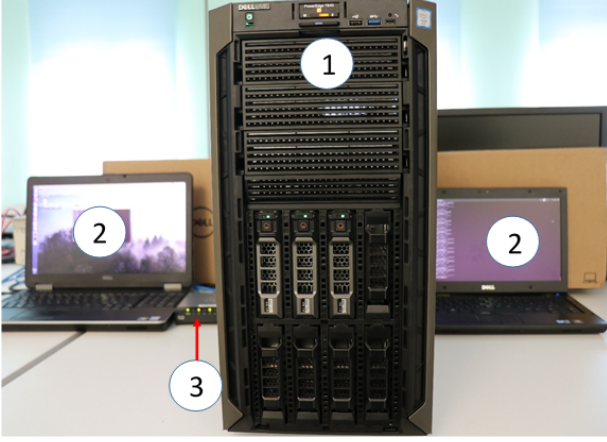


Fig. 9. Testbed setup. (1) Dell T640 server (2) Client PCs (3) Gbps switch.

In order to evaluate the effectiveness of our scheme we run experiments on a test-bed that mirrors the operations of a CSP. We setup the test-bed as shown in Fig. 9. The processor architecture of our Dell T640 server consists of two processor sockets with Non Uniform Memory Allocation (NUMA), 10 hyper-threaded CPU cores per socket for a total of 40 logical cores with a variable clock rate. The server memory is 128 GB.

The server runs Ubuntu 18.04 LTS as its operating system and acts as a host for virtual machines which run the cloud application. The Client PCs run Ubuntu 16.04.3 LTS as their operating system. We use KVM as the hypervisor and manage the virtual machines using libvirt [25]. Each instance of a virtual machine is configured with 4 virtual CPUs and 4 GB of memory. We connected a set of PCs to the server via a Cisco switch to form a Gigabit/s local area network. The PCs function as ASPs running bash scripts that generate requests to the server with varying rates as depicted in Figs. 10 and 11.

The server launches VMs to handle incoming requests according to the different schemes compared in this work: static provisioning, extended Kalman filtering based prediction and SQLR. All schemes including the admission control and load balancer VNFs are implemented in Python and are run within the host.

As mentioned in Section 2, the state-of-the-art scheme in [10] leverages a queuing system model enhanced with an Extended Kalman Filter (EKF). It makes near time predictions of response times based on measurements of arrival

rates and system utilization. Using a queue model refined by a tuned EKF with the maximum allowable response time (from an SLA) as input, it then calculates the number of nodes needed and scales appropriately to get to this number.

We make some slight modifications to the algorithm to make it more robust. We increase the interval between the predict and update phases from 10s to 90s as this provides sufficient time for starting up a VM node and letting it handle traffic. Additionally, we use the average values (taken over the predict and update interval of the EKF) as opposed to the instantaneous measured values of system utilization and response times as inputs to the EKF. This prevents the scaler from over/under estimating input parameters and thus presents a fairer comparison to SQLR. Further we dispense with the network delay in the system model as the response times are taken directly on the server. We consider only a single-tiered application, and only one class of requests. This also has the effect of simplifying the process and measurement noise covariance matrices to $\mathbb{R}^{2 \times 2}$ (as only two parameters are taken into account in each case) thereby improving the tuning of the EKF.

For the SQLR case, in order to reduce the state space as well as the associated number of episodes required for convergence, we limit the maximum number of virtual machines that can be added or removed to 2 for our experiments. In addition, we employ a damping mechanism which (for the fully converged states) requires two consecutive scale-in decisions before withdrawing resources. The latter ameliorates premature removal of resources while allowing expedited provisioning to handle sudden increases in demand.

As stated earlier, we use the bitcoin proof-of-work computation as our test cloud application. We limit the number of iterations generated by a request to specific target values so as to mimic the varying degrees of complexity of typical cloud application requests. The number of hash operations generated by a request comes from the discrete set $\{300k, 400k, \dots, 1200k\}$.

As part of the training for the SQLR elastic provisioning system, we combined several traffic profiles with various workload averages resulting in the composite shown in Fig. 10.

For the test traffic we again used a combination of several profiles with different workload averages to obtain the composite shown in Fig. 11. To achieve this we configured requests to be sent with inter-arrival times with the discrete distribution $\lambda \sim \mathcal{U}\{0, \lambda_{\max}\}$ for each hour slot. For example for the busy-hour slot $\lambda_{\max} = 5s$ and the for low traffic period $\lambda_{\max} = 9s$. This results in high entropy (given the uniform distribution of inter-arrival times) and presents greater stochastic behaviour which is more challenging than those encountered in common reference profiles as those used in [10]. Moreover, it exhibits patterns encountered in real workloads with rapid variations over short intervals but with veritable trends over longer observation windows. It also includes sudden bursts and drops such as those observed at the start of hour 7, 10, 14 and 18. We run multiple instances of the admission control and load balancer functions on different ports (which increases workload averages for the constituent profiles by leveraging volume instead of frequency of arrivals) in order to reduce port binding errors

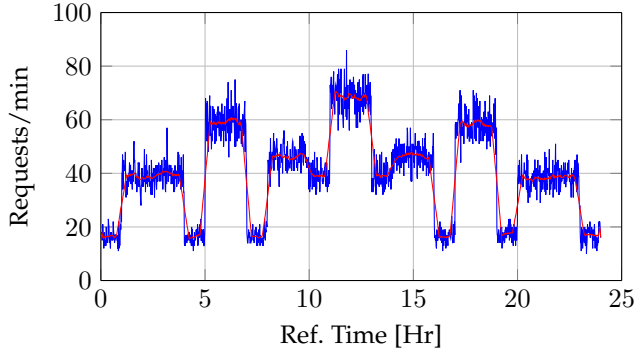


Fig. 10. Pre-training workload profile. The red line is the moving average of requests with a window of 30 samples.

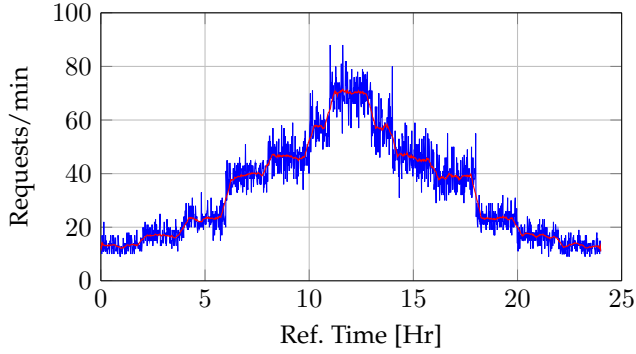


Fig. 11. Test workload profile. The red line is the moving average of requests with a window of 30 samples.

at the server side.

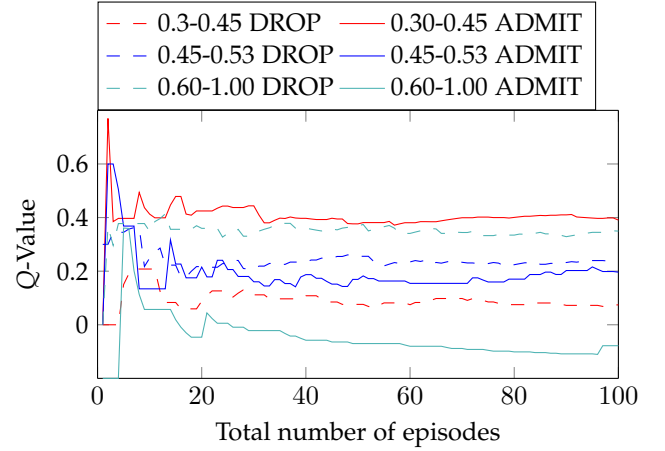
5 RESULTS

In this section, we show the effectiveness of policy convergence leveraging the results from the training of the admission control function. We then examine the results of with respect to two SLOs: service availability (as measured via blocking rates) and service times.

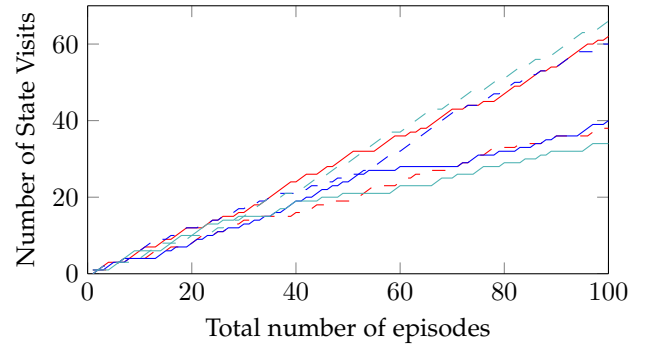
5.1 Admission control

We briefly discuss our admission control function which learns the appropriate utilization limit to apply in its policy to ensure that response times are reliably bounded.

Fig. 12 shows how the learning algorithm for the admission control trades off exploration and exploitation using our weighted fair exploration scheme (7). The evolution of the accumulated reward for 3 state-action pairs is shown in Fig. 12a. In the initial learning phases, the difference between the values is not as distinct and a DROP or ADMIT decision is made with largely the same probability. However as the admission control continues to update the accumulated reward values at every episode, the comparative value in each state-action pair becomes more distinct. The latter results in more ADMIT than DROP decisions in the regions spanning the lower utilization levels, and the converse in the regions spanning the high utilization levels as shown in Fig. 12b.



(a) Reward accumulated with experience.



(b) Frequency of DROP and ADMIT decisions.

Fig. 12. Admission Control training. At the onset, the cumulative rewards are closer together and decisions are more equi-probable. As the agent makes more decisions over subsequent episodes, the admission policy for each of the states becomes more distinct, and weighted fair exploration favors the actions with higher rewards.

At convergence the admission policy for each region is fully determined. Strong ADMIT and strong DROP policies are at the extreme levels of low and high utilization respectively. In the mid levels of utilization, the difference in the decision variable (Q-Value) is not as stark resulting in a weak drop decision at the boundary.

The limiting value of utilization x_{lim} , beyond which service times are generally unpredictable, is learned to be 45%. The admission controller therefore drops requests sent to a selected VM whose utilization is higher than this value. We recall that load balancer selects the VM with the lowest utilization value at the time of receiving a request.

5.2 Horizontal Scaling

The scaling profile obtained against the composite test traffic profiles for the horizontal scaling scheme proposed in [10], with target response time $R_{sla} = 5 \mu s$ per proof-of-work iteration, is shown in Fig. 13. The scaling behaviour of this scheme is quite stiff given its reliance on workload measurements which may filter out bursty traffic that require greater agility.

The scaling profile from our proposed SQLR scheme is shown in Fig. 14. The behaviour of the scaler steadily improves with increased exposure to the test traffic. As more states converge, as seen by moving from Fig. 14a

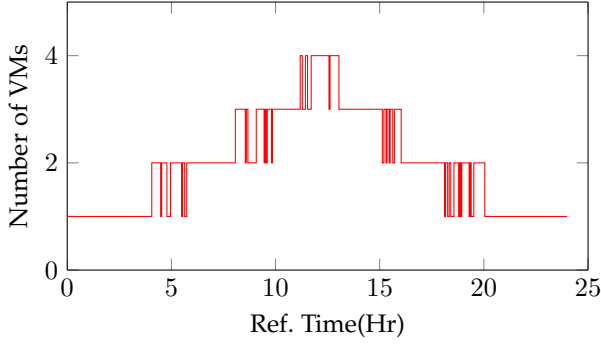


Fig. 13. VM Scaling for the EKF-based horizontal scaling scheme proposed in [10].

to Fig. 14b and Fig. 14c, the scaling behaviour becomes more predictable. The number of VMs provisioned oscillates about a suitable number that best achieves the compromise of resource cost and penalties encapsulated in the training parameters θ and β .

Moreover, in Fig. 14b, we see that the first intervals to exhibit convergence (implied by greater stability in the scaling behaviour) are those with higher similarity to the training traffic. An example of this are the intervals between hours 6 and 8 as well as hours 16 and 18 with 40 requests per minute. These closely resemble intervals of the training traffic between hours 1 and 4 and between hours 20 and 23 of the test traffic shown in Fig. 10. This shows the ability of SQLR to re-use contextual knowledge learned from one workload on a subsequent one with similar characteristics.

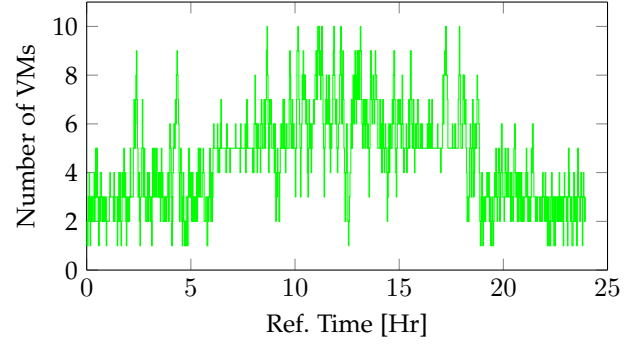
Assigning different values to the training parameters θ and β results in different policies being learned by SQLR. As shown in Fig. 14c, a low value of θ relative to β (Case 1) results in conservative scaling policies that emphasize resource cost more than service unavailability due to blocking. When $\theta \gg \beta$, as in Case 2, more liberal policies are learned giving greater importance to service availability than to resource cost.

5.3 Blocking Rates

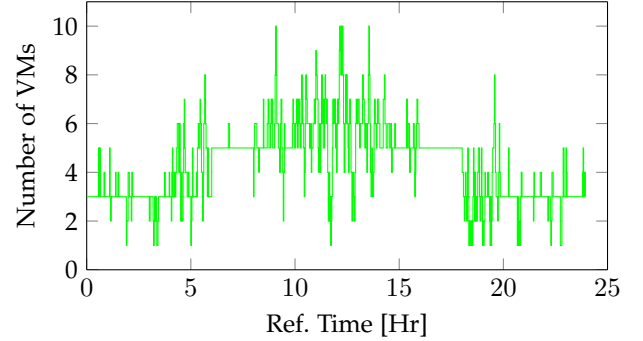
The exploration mechanism of the Q-Learning algorithm at the core of SQLR means that it may sometimes make sub-optimal decisions in less known states, resulting in under-provisioning (such as at hour 18 for case 1 and hour 5 for case 2 in Fig. 14c). This results in relatively high blocking rates as shown in Fig. 15. Our guided fair exploration mechanism ameliorates the effects of such under-provisioning ensuring that their duration is short.

Since the EKF scaler relies on workload measurements to predict response times and scale accordingly, it is particularly susceptible to under-estimating resource requirements when demand is low. This is evident at off-peak intervals in Fig. 15 where, between hours 0 and 7 and between hours 17 and 24 it averages an allocation of 1 VM resulting in considerable blocking much higher than the other schemes.

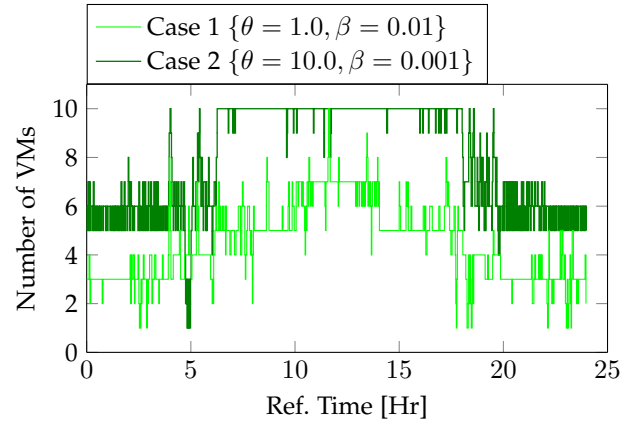
Static provisioning results in significant under- or over-provisioning, as exhibited by the 2 VMs and 10 VMs curves respectively. This situation is clearly untenable given that serious penalties are levied on the CSP for service unavailability on the one hand; and on the other hand, significant yet



(a) At approx. 10% convergence. With $\theta = 1.0$, $\beta = 0.01$.



(b) At approx. 20% convergence. With $\theta = 1.0$, $\beta = 0.01$. Early stabilization from 6-8 and 16-18 is due to the similarity of the workload experienced in these regions with that of the training traffic profile.



(c) At approx. 50% convergence.

Fig. 14. SQLR scaling behaviour with experience after pre-training with $\bar{P} = 0.001$. The convergence level is the proportion of unique states visited for which $\epsilon = \epsilon_{\min}$.

unnecessary operational expenditure is incurred to maintain superfluous resources.

Fig. 16 compares the distribution of blocking rates for the provisioning mechanisms. Taking the static over-provisioned case as a reference benchmark with no blocking and resources in terms of VM-hours; SQLR Case 2 saves up to 25% of resources with less than 5% blocking for 99% of the requests. SQLR Case 1 saves up to 55% of resources with less than 5% blocking for 92% of the requests. The EKF-based scaler saves almost 80% VM-Hours but at the expense of service availability, only 65% of the requests are served with less than 5% being blocked. The static

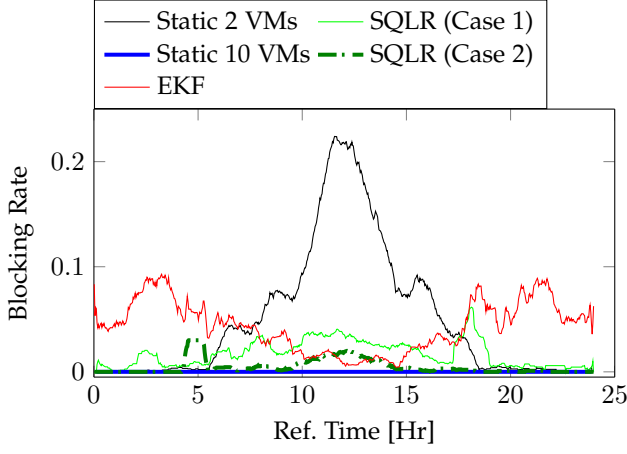


Fig. 15. Blocking rates over two-minute intervals. Two SQLR configurations are shown: Case 1 ($\theta = 1.0, \beta = 0.01$) and Case 2 ($\theta = 10.0, \beta = 0.001$). For clarity, a moving average filter is applied with a window size of 30 samples.

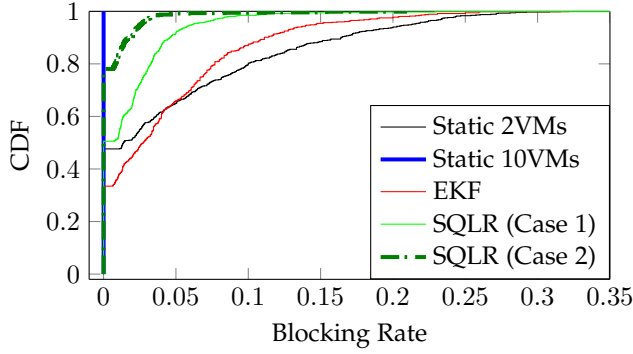


Fig. 16. Blocking rate distribution. Two SQLR configurations are shown: Case 1 ($\theta = 1.0, \beta = 0.01$) and Case 2 ($\theta = 10.0, \beta = 0.001$).

under-provisioned case of 2 VMs achieves similar savings as the EKF-based scaler with similar performance at the 5% blocking reference. However, when we consider requests with up to 10% blocking, the EKF-based scaler only achieves this for 80% of the requests but static provisioning with 2 VMs achieves this for 88% of the requests.

5.4 Service times

The distribution of service times is shown in Fig. 17. We obtain the service time per proof-of-work iteration by dividing the service time of each request by the corresponding number of iterations it generates. These response times include the administrative overhead incurred by the hypervisor in switching between guest and host operating system's user mode and kernel mode in managing virtual machines as mentioned in our previous work [21]. This cost increases with the number of virtual machines being administered as well as with how often they change state. Dynamic scaling which entails switching VM Nodes on and off contributes to the latter. Owing to this, the second SQLR policy (with greater penalties for blocking than resource use) is impacted greatly by this phenomenon as its policies implicitly employ more VMs. It closely follows the static over-provisioned

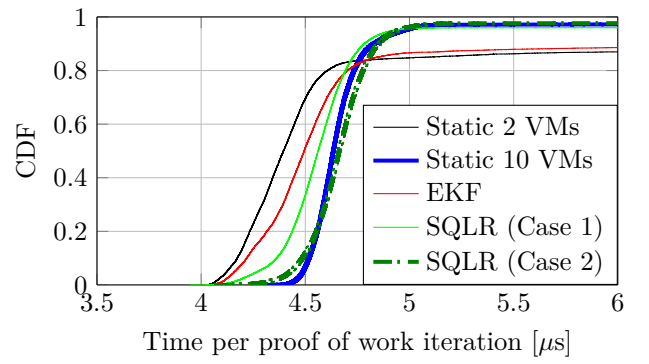


Fig. 17. Service time distribution per proof-of-work iteration. Two SQLR configurations are shown: Case 1 ($\theta = 1.0, \beta = 0.01$) and Case 2 ($\theta = 10.0, \beta = 0.001$). The service time for each request is divided by the corresponding number of iterations it generates to obtain the time per proof-of-work iteration.

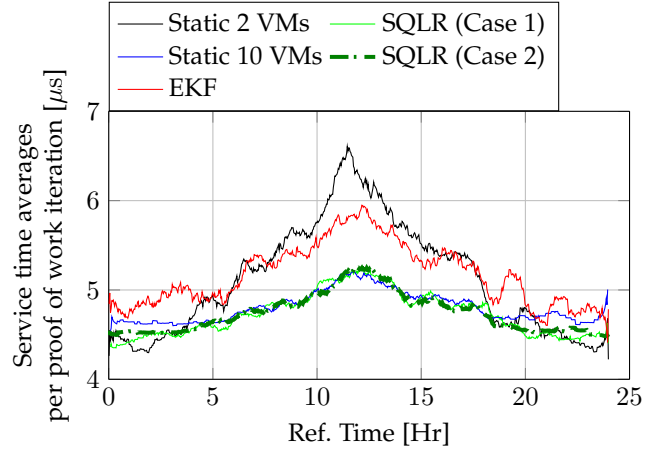


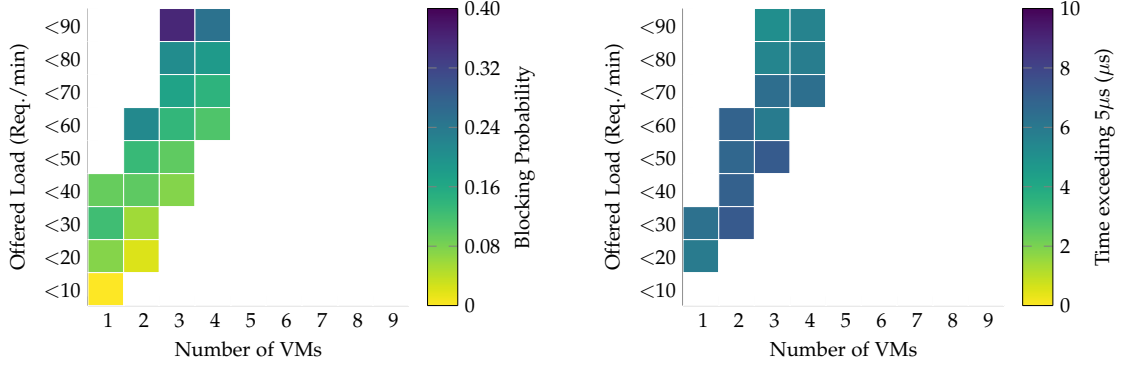
Fig. 18. Moving averages of service times (taken over a window of 30 samples to smooth out switching overheads). Two SQLR configurations are shown: Case 1 ($\theta = 1.0, \beta = 0.01$) and Case 2 ($\theta = 10.0, \beta = 0.001$).

case with 10 VMs which has a persistently high switching overhead.

However, the over-provisioned scenario still provides the ideal case with the lowest variance (highly predictable) service times. Both SQLR schemes closely approach this ideal case with about 96% of the requests being served within $5 \mu s$ per proof-of-work iteration compared to 94% for the over-provisioned case and only 87% for the EKF case.

Moreover, for SQLR with $\theta = 10.0$ and $\beta = 0.001$, the improvement in the proportion of responses within the cut-off service time of $5 \mu s$ is marginal, given the extra amount of resources it assigns, compared to the more conservative case with $\theta = 1.0$ and $\beta = 0.01$ as shown in Fig. 14c. This represents a diminishing return on policies biased to provision more VMs, owing primarily to the additional administrative cost as described above.

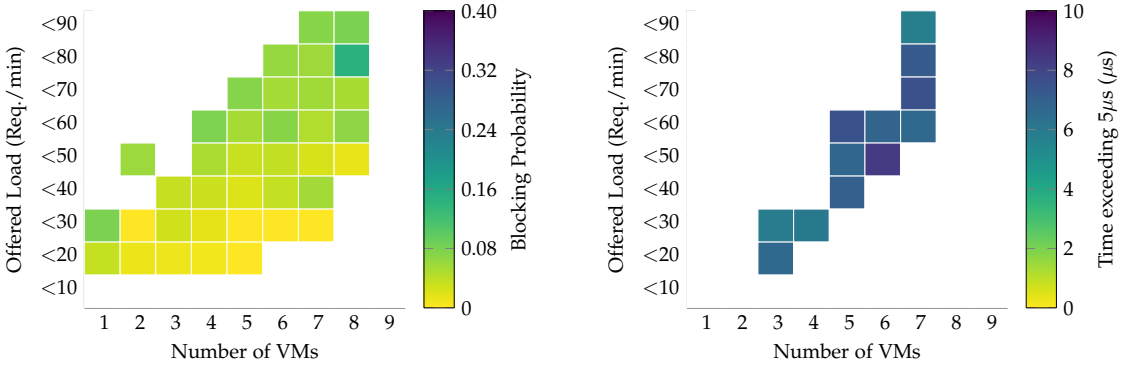
We average out the effect of this system overhead, which is akin to noise in communication systems, in order to reduce its bias on the results. We do this by first obtaining the average service times over two-minute intervals and then applying a moving average filter having a window of



(a) Frequency of blocking. The number of responses exceeding $5 \mu s$ as a fraction of the total number of responses. The white region indicates unexplored resource allocations for the offered load.

(b) Severity of blocking. The mean deviation from $5 \mu s$ of the responses exceeding $5 \mu s$. The white region includes responses within the service time limit as well as unexplored allocations.

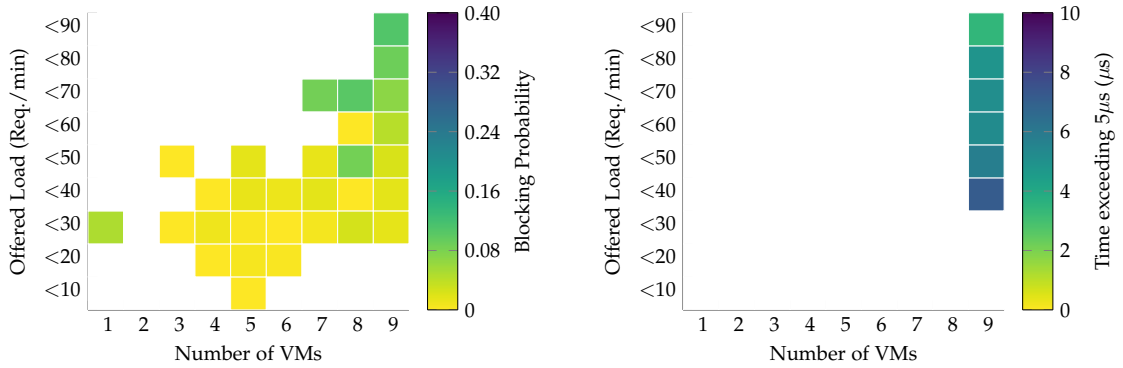
Fig. 19. Soft Blocking Probability for EKF Scaler. 87% of the responses are within $5 \mu s$ per proof-of-work iteration. Only blocks with statistical significance (30 or more responses) are considered.



(a) Frequency of blocking. The number of responses exceeding $5 \mu s$ as a fraction of the total number of responses. The white region indicates unexplored resource allocations for the offered load.

(b) Severity of blocking. The mean deviation from $5 \mu s$ of the responses exceeding $5 \mu s$. The white region includes responses within the service time limit as well as unexplored allocations.

Fig. 20. Soft Blocking Probability for SQLR Case 1 ($\theta = 1.0$, $\beta = 0.01$). 95.6% of the responses are within $5 \mu s$ per proof-of-work iteration. The instances of high severity are mainly due to exploratory scale-in actions in states where $\epsilon > \epsilon_{\min}$. Only blocks with statistical significance (30 or more responses) are considered.



(a) Frequency of blocking. The number of responses exceeding $5 \mu s$ as a fraction of the total number of responses. The white region indicates unexplored resource allocations for the offered load.

(b) Severity of blocking. The mean deviation from $5 \mu s$ of the responses exceeding $5 \mu s$. The white region includes responses within the service time limit as well as unexplored allocations.

Fig. 21. Soft Blocking Probability for SQLR Case 2 ($\theta = 10.0$, $\beta = 0.001$). 96.2% of the responses are within $5 \mu s$ per proof-of-work iteration. The instances of high severity are mainly due to exploratory scale-in actions in states where $\epsilon > \epsilon_{\min}$. Only blocks with statistical significance (30 or more responses) are considered.

30 samples. Since context switching happens in the order of clock cycles, these two operations over intervals that are orders of magnitude longer than a clock cycle nearly nullify switching effects.

When we apply the operations stated above to the service time per proof-of-work iteration, we obtain the results depicted in Fig. 18. Both SQLR cases considered, closely follow the over-provisioned one with the ideal response times. At low traffic (hours 0-7 and 17-24), the administrative costs for maintaining a large number of VMs outweigh the gains made in improving service times by using more resources. Over these intervals, SQLR performs slightly better than the unconstrained case by provisioning fewer VMs. However, the EKF-based scaler still under-performs since the single VM it provisions over these intervals is not sufficient to meet the demand within the cut-off service time. This marked difference in response times owing to the differences in the scaling mechanisms is clearly depicted in Figs. 19 to 21 where we compare the soft-blocking performance (defined as the proportion of accepted requests whose service times extend beyond our cut-off of 5 μ s per proof-of-work iteration). In these heatmaps, the white region indicates unexplored resource allocations for the offered load and, additionally for the severity heatmaps in Figs. 19b, 20b and 21b, those allocations leading to service times within the limit of 5 μ s. Moreover, the offered load values on the y-axis indicate the upper bound with the value immediately below indicating the lower bound i.e. "<20" indicates the interval [10,20) requests per min.

As depicted in Fig. 19, the EKF scaler employed by [10] is prone to overruns even under light loads given that it is very conservative in allocating extra VMs. As a result, this increases the strain on the few that are assigned. In our scheme, whose responses are shown in Figs. 20 and 21, a smaller proportion of service times exceed the cut-off time (particularly at moderate to high offered loads). The reason is that SQLR is more sensitive to abrupt changes in traffic and assigns resources in a more agile fashion compared to the EKF-based scheme. In fact, the latter leverages average workload measurements to make scaling decisions, and is thereby oblivious to short-lived bursts in demand.

Further comparing the SQLR cases shown in Figs. 20 and 21, the liberal provisioning policies of Case 2 result in fewer instances of soft blocking than Case 1. The reason is that traffic distribution among fewer VMs increases the likelihood of operating them at higher CPU loads hence longer service times as alluded to in (8), the converse is true for more VMs. The cases of high severity (particularly in Case 2) are because of exploratory actions at high demand whereby SQLR momentarily scales in. However, by evaluating the sub-optimality of this action, using our weighted fair guided exploration, quickly scales out as is evident around hours 10 and 12 in Fig. 14c.

6 CONCLUSIONS AND FUTURE WORK

We have presented an agile horizontal scaling system, SQLR, that learns the most appropriate horizontal scaling decision to take (without any fore-knowledge of the underlying system configuration) under highly dynamic workloads. We show that our modified Q-Learning scheme

enables our system to learn multiple policies and transfer any applicable knowledge to new traffic profiles exhibiting previously encountered characteristics.

SQLR progressively self optimizes resource cost and service availability constraints to achieve the proper trade-off. These constraints can be supplied by the CSP as external input after proper determination from their business process. Such high-level objectives makes SQLR easily configurable and adaptable to any cloud application as no domain-specific knowledge is required. We contrast this with a state-of-the-art scaling system and show that our scheme achieves superior performance similar to that of an over-provisioned system.

As with most artificial intelligence systems, our scheme is subject to a training overhead. However, because of its capacity for contextual knowledge re-use, it can be trained offline with representative workloads. Also given our weighted fair exploration mechanism, any subsequent residual learning can be done in production workloads with a much reduced risk of poor decisions in the process. We show that with only about 50% of fully converged states, our scheme performs almost as well as the unconstrained resource benchmark (static over-provisioning).

In the future, we intend to apply the short-term memory Q-Learning employed in this work to migrate VM nodes to other hosts when the physical resources of the active host are under strain. We also plan to use a variant of the scheme to carry out orchestration of distributed cloud applications.

REFERENCES

- [1] J. Anselmi, D. Ardagna, J. C. S. Lui, A. Wierman, Y. Xu, and Z. Yang, "The economics of the cloud," *ACM Trans. Model. Perform. Eval. Comput. Syst.*, vol. 2, no. 4, Aug. 2017.
- [2] C. Wang, B. Urgaonkar, G. Kesidis, A. Gupta, L. Y. Chen, and R. Birke, "Effective capacity modulation as an explicit control knob for public cloud profitability," *ACM Trans. Auton. Adapt. Syst.*, vol. 13, no. 1, May 2018.
- [3] P. Cong, L. Li, J. Zhou, K. Cao, T. Wei, M. Chen, and S. Hu, "Developing user perceived value based pricing models for cloud markets," *IEEE Transactions on Parallel and Distributed Systems*, vol. 29, no. 12, pp. 2742–2756, Dec 2018.
- [4] "Rightscale," <https://www.rightscale.com>, accessed: 2019-03-07.
- [5] "EC2, elastic compute v2," <https://aws.amazon.com/ec2>, accessed: 2019-03-07.
- [6] S. Farokhi, E. B. Lakew, C. Klein, I. Brandic, and E. Elmroth, "Coordinating cpu and memory elasticity controllers to meet service response time constraints," *Proc. International Conference on Cloud and Autonomic Computing*, pp. 69–80, 2015.
- [7] M. Z. Hasan, E. Magana, A. Clemm, L. Tucker, and S. L. D. Gudreddi, "Integrated and autonomic cloud resource scaling," *Proc. IEEE Network Operations and Management Symposium*, pp. 1327–1334, 2012.
- [8] P. Jamshidi, A. Ahmad, and C. Pahl, "Autonomic resource provisioning for cloud-based software," *Proc. International Symposium on Software Engineering for Adaptive and Self-Managing Systems*, 2014.
- [9] A. Alsarhan, A. Itradat, A. Y. Al-Dubai, A. Y. Zomaya, and G. Min, "Adaptive resource allocation and provisioning in multi-service cloud environments," *IEEE Transactions on Parallel and Distributed Systems*, vol. 29, no. 1, pp. 31–42, Jan 2018.
- [10] A. Gandhi, P. Dube, A. Karve, A. Kochut, and L. Zhang, "Model-driven Optimal Resource Scaling in Cloud," *Softw. Syst. Model.*, vol. 17, no. 2, May 2018.
- [11] N. Vasić, D. Novaković, S. Miućin, D. Kostić, and R. Bianchini, "Dejavu: Accelerating resource allocation in virtualized environments," *SIGARCH Comput. Archit. News*, vol. 40, no. 1, Mar 2012.
- [12] O. Ibadunmoye, M. H. Moghadam, E. B. Lakew, and E. Elmroth, "Adaptive service performance control using cooperative fuzzy reinforcement learning in virtualized environments," in *Proc. International Conference on Utility and Cloud Computing*, 2017.

- [13] J. Liu, Y. Zhang, Y. Zhou, D. Zhang, and H. Liu, "Aggressive resource provisioning for ensuring qos in virtualized environments," *IEEE Transactions on Cloud Computing*, vol. 3, no. 2, pp. 119–131, April 2015.
- [14] H. Fernandez, G. Pierre, and T. Kielmann, "Autoscaling web applications in heterogeneous cloud infrastructures," *Proc. IEEE International Conference on Cloud Engineering*, pp. 195–204, March 2014.
- [15] P. Leitner, W. Hummer, B. Satzger, C. Inzinger, and S. Dustdar, "Cost-Efficient and Application SLA-Aware Client Side Request Scheduling in an Infrastructure-as-a-Service Cloud," *Proc. IEEE International Conference on Cloud Computing*, pp. 213–220, June 2012.
- [16] J. Mei, K. Li, Z. Tong, Q. Li, and K. Li, "Profit maximization for cloud brokers in cloud computing," *IEEE Transactions on Parallel and Distributed Systems*, vol. 30, no. 1, pp. 190–203, Jan 2019.
- [17] Q. Wang, Y. Kanemasa, M. Kawaba, and C. Pu, "When Average is Not Average: Large Response Time Fluctuations in N-tier Systems," *Proc. International Conference on Autonomic Computing*, pp. 33–42, 2012.
- [18] S. Nakamoto, "Bitcoin: A peer-to-peer electronic cash system," Dec 2008, accessed: 2019-07-03. [Online]. Available: <https://bitcoin.org/bitcoin.pdf>
- [19] J. Li, J. Li, X. Chen, C. Jia, and W. Lou, "Identity-based encryption with outsourced revocation in cloud computing," *IEEE Transactions on Computers*, vol. 64, no. 2, pp. 425–437, Feb 2015.
- [20] X. Li, M. A. Salehi, Y. Joshi, M. K. Darwich, B. Landreneau, and M. Bayoumi, "Performance analysis and modeling of video transcoding using heterogeneous cloud services," *IEEE Transactions on Parallel and Distributed Systems*, vol. 30, no. 4, pp. 910–922, April 2019.
- [21] C. Ayimba, P. Casari, and V. Mancuso, "Adaptive Resource Provisioning based on Application State," *Proc. International Conference on Computing, Networking and Communications*, pp. 663–668, Feb 2019.
- [22] C. J. C. H. Watkins, "Learning from delayed rewards," Ph.D. dissertation, King's College, Cambridge, UK, May 1989.
- [23] R. S. Sutton and A. G. Barto, *Introduction to Reinforcement Learning*, 1st ed. Cambridge, MA, USA: MIT Press, 1998.
- [24] L. Kleinrock, "Time-shared systems: A theoretical treatment," *Journal of the ACM*, vol. 14, no. 2, Apr. 1967.
- [25] M. Bolte, M. Sievers, G. Birkenheuer, O. Niehörster, and A. Brinkmann, "Non-intrusive Virtualization Management Using Libvirt," in *Proc. Design, Automation Test in Europe*, Leuven, Belgium, Mar 2010.

Paolo Casari received the PhD in Information Engineering in 2008 from the University of Padova, Italy. He was on leave at the Massachusetts Institute of Technology in 2007, working on underwater communications and networks. He collaborated to several funded projects including CLAM (FP7), RACUN (EDA), as well as US ARO, ONR and NSF initiatives. He is the PI of the NATO SPS project ThreatDetect, and the scientific coordinator of the EU H2020 RECAP and SYMBIOSIS projects. In 2015, he joined the IMDEA Networks Institute, Madrid, Spain, where he leads the Ubiquitous Wireless Networks group. He regularly serves in the organizing committee of several international conferences, and is currently on the editorial boards of the *IEEE Transactions on Mobile Computing* and of the *IEEE Transactions on Wireless Communications*. Previously, he has been guest editor of a special issue of *IEEE Access* on Underwater Acoustic Communications and Networking, as well as of a special issue of the *Hindawi Journal of Electrical and Computer Engineering* on the same topic. He received two best paper awards. His research interests include many aspects of networked communications, such as channel modeling, network protocol design, localization, simulation, and experimental evaluations.

Vincenzo Mancuso is Research Associate Professor at IMDEA Networks Institute, Madrid, Spain, and recipient of a Ramon y Cajal research grant of the Spanish Ministry of Science and Innovation. Previously, he was with INRIA Sophia Antipolis (France), Rice University (Houston, TX, USA) and University of Palermo (Italy), from where he obtained his MSc and his Ph.D. in Electronics, Computer Science and Telecommunications. He has authored more than 110 peer-reviewed publications focusing on Internet QoS and on the analysis, design, and experimental evaluation of opportunistic and adaptive protocols and architectures for wireless networks. He is currently working on analysis and optimization of wireless access networks and on the measurements and assessment of mobile broadband networks.

Constantine Ayimba received his M.Sc. in Wireless Communications from Lund University (Sweden) in 2016 where he was a Swedish Institute Scholar. He previously held positions in Ericsson and Strathmore University (Kenya). He obtained his BSc. in Electrical Engineering from the University of Nairobi (Kenya) in 2006. He is currently pursuing his Ph.D. at IMDEA Networks Institute (Spain) where his research focuses on machine learning for self-driving networks.